Title

CHEMISORPTION GEOMETRY OF c(2x2)S/Mo(001) DETERMINED WITH ANGLE-RESOLVED PHOTOEMISSION EXTENDED FINE STRUCTURE

Author

Bahr, C.C.

Publication Date

1986-05-01

Lawrence Berkeley Laboratory
UNIVERSITY OF CALIFORNIA

Materials & Molecular Research Division

Submitted to Physical Review B

CHEMISORPTION GEOMETRY OF c(2x2)S/Mo(001) DETERMINED WITH ANGLE-RESOLVED PHOTOEMISSION EXTENDED FINE STRUCTURE

C.C. Bahr, S.W. Robey, Z. Hussain, L.J. Terminello, K.T. Leung, J.-R. Lou, A.E. Schach von Wittenau, and D.A. Shirley

May 1986

Prepared for the U.S. Department of Energy under Contract DE-AC03-76SF00098

DISCLAIMER

LBL-21221

Chemisorption Geometry of c(2x2)S/Mo(001) Determined with Angle-Resolved Photoemission Extended Fine Structure

C.C. Bahr, S.W. Robey, Z.Hussain,* L.J. Terminello, K.T. Leung, Ji-Ren Lou, A.E. Schach von Wittenau, and D.A. Shirley

Materials and Molecular Research Division,
Lawrence Berkeley Laboratory
and
Departments of Chemistry and Physics,
University of California,
Berkeley, CA 94720

Abstract

We report the chemisorption geometry for c(2X2)S/Mo(001), as determined using angle-resolved photoemission extended fine-structure (ARPEFS). Sulfur is bonded as expected to the fourfold hollow sites, with a S-Mo bond distance of 2.41(2)Å. The Mo first-to-second layer spacing is within 0.03Å of the bulk spacing and the second Mo layer is planar within 0.03Å. We determined the adsorption geometry of sulfur by fitting ARPEFS curves with a multiple-scattering spherical-wave theory, which provided good agreement with the data.

I. Introduction

Photoelectron diffraction (PD) is the interference of the different paths of a photoelectron from the emitting atom to the detector. One path is direct, and accounts for most of the amplitude at the detector. Other paths include one or more scattering events off nearby atoms; each path has a unique length related to the scattering angle and the distance from the emitter to the scatterer. The difference in path lengths introduces a wavelength-dependent phase shift between the direct path and a scattered path. The total phase shift Φ is given by

$$\Phi = kr (1 - \cos\theta) + \phi(k,\theta),$$

where k is the photoelectron momentum, r is the distance from the emitter to the scatterer, θ is the scattering angle (0° = no deflection), and ϕ is the additional phase shift introduced by the scattering atom. We measure photoelectron diffraction as a function of photon energy over a wide enough range (~500 eV) so that we can extract semi-quantitative structural information directly as in extended x-ray absorption fine structure (EXAFS) and hence our acronym ARPEFS, angle-resolved photoemission extended fine-structure.

ARPEFS analysis has been developed to the point where detailed chemisorption geometries can be routinely measured with high accuracy. The application of theory to the extraction of subtle surface-relaxation and reconstruction effects is time-consuming,[1,2] yet

provides the ultimate three-dimensional probe of the local atomic environment of a surface adsorbate.

The chemisorption of sulfur on molybdenum has attracted attention because of the catalytic activity of MoS_2 in dehydrosulfurization reactions.[3] The clean Mo surface is relaxed (13% contraction),[4] and it reconstructs below room temperature[5]. The relaxation disappears upon silicon adsorption.[6] Ion-scattering[7] results suggest that sulfur adsorbs in the fourfold hollow site ~1Å above the Mo surface, in agreement with earlier low energy electron diffraction (LEED) results.[8] None of the experiments measured a precise adsorption geometry.

We describe here the measurement and analysis of ARPEFS from the 1s level of sulfur adsorbed in a c(2X2) symmetry on Mo(001). Details of the ARPEFS measurement are presented in Section II. Data reduction is described in Section III, and the subsequent extraction of structural parameters, such as the S-Mo bond length and the Mo layer spacing, is described in Section IV. Results are discussed in Section V.

II. Experimental

A (2mm thick X 6mm dia.) crystal was oriented to within 0.5° of (001) and polished to a mirror finish (final polish, 0.05μm Al_2O_3). The Mo was cleaned using three methods: room temperature Ar^+ bombardment (~1000eV), annealing with oxygen (700-1400K, $1X10^{-8}$- $1X10^{-6}$ torr O_2), and annealing in vacuum (≤2000K). We checked the effectiveness of the cleaning procedure using Auger electron spectroscopy (AES) and LEED.

Following several cycles of Ar^+ bombardment and annealing, the major contaminant was carbon. We then exposed the crystal to ~$1X10^{-7}$ torr oxygen for several hours at 1500K to burn out the carbon. The surface carbon was gone, but removal of the surface oxide required several sputtering and annealing cycles. As the oxygen disappeared, the carbon reappeared. We could adjust the annealing cycles to produce a surface apparently free of both carbon and oxygen, as judged by AES. A c(2X2) sulfur overlayer was prepared on this surface for the curve labeled #1 in Fig. 3. The sulfur overlayer was made by exposing the surface to ~1L ($L=10^{-6}$ torr sec) H_2S and gently heating to ~500K. The LEED patterns we obtained for the clean and sulfur-covered surface were a sharp (1X1) and a moderately sharp c(2X2), respectively. The subsequent ARPEFS curves were measured after an improved cleaning method. High temperature annealing cycles (2000K) and moderate oxygen treatments ($1X10^{-8}$ torr at 1000K for 30 sec) released the residual bulk carbon impurity so that additional annealing did not segregate carbon to the surface. The clean and sulfur covered surfaces prepared from the improved recipe had sharper LEED spots with a lower background, indicative of fewer surface defects. Following the ARPEFS measurements (~36 hours in vacuum) the LEED background increased considerably, but c(2X2) spots were still clearly visible. After the measurement of the 0° curve #1, some additional fuzzy spots were present near p(4X4) positions.

We measured the ARPEFS curves at the Stanford Synchrotron Radiation Laboratory (SSRL) on the Jumbo beam line,[9] which provided photons through the energy range 2500 eV $\leq h\nu \leq$ 3000 eV, with a resolution of ~2 eV. Electron spectra were collected with a

multichannel angle-resolved electron spectrometer[10] operated at a pass energy of 160 eV, giving a resolution of ~1 eV. We collected ca. 70 spectra at different photon energies for each ARPEFS curve. Electron spectra were normalized to a constant photon flux with a Ni grid and channeltron situated between the x-ray monochromator and the sample. The total measuring time for each ARPEFS curve was 12-24 hours.

The sample was oriented in two positions for these measurements. The 0° data were collected with the electron analyzer aligned along the [001] direction, or the surface normal, as shown in Fig. 1. For these curves the polarization vector was tilted 35° from the surface normal, towards [111]. The 35° measurements were made with the electron analyzer and the polarization vector aligned with the 35° vector, also shown in Fig. 1.

III. Data Reduction.

We must process over 70 photoelectron spectra to obtain a single ARPEFS curve. This is necessary because the adsorbate photoemission lines ride on a high background which would otherwise obscure the PD effect. We have previously[1,2] described the data reduction for ARPEFS. S/Mo is a difficult system to be studied by ARPEFS, but other, more conventional surface EXAFS methods would be even more difficult because of the Mo absorption edges which lie in the energy range of interest as discussed below. We will discuss three aspects of the data reduction for S/Mo: peak fitting, normalization, and removal of the atomic-like background I_0.

Peak/curve fitting is necessary to separate the full-energy photoelectron peak from other structures, such as Auger peaks, e.g., Mo MNN peaks. In earlier experiments with Cu[2] and Ni,[1] the interfering Auger peaks were not significant because they had low intensity or fell outside the ARPEFS energy range (~80-550eV). The Mo MNN Auger peaks occur in the middle of the ARPEFS range and are of intensity comparable to that of the photoemission line. An example of the interfering Auger peaks is shown in Fig. 2, where typical electron spectra are plotted in the photon energy range, 2682 eV to 2706 eV. The constant kinetic energy peaks are Mo MNN Auger peaks and the constant binding energy peak, or the narrow peak which moves with photon energy, is the S 1s peak.

We fit the spectra in the complicated Auger region with only three functions: a Gaussian peak (photoelectron peak), a Gaussian-broadened step function (inelastically-scattered photoelectrons), and a background template. The background template for a specific spectrum "I" was formed by making a first-pass fit to the spectra above, "I+1", and below, "I-1", in photon energy. The first-pass fit was used to remove the photoelectron contribution to the "I+1" and "I-1" spectra. The peak subtracted spectra were then overlaid and averaged to approximate the background of the "I" spectrum. Then the "I" spectrum was fitted with the three functions: peak, step, and background template. Using the empirically-determined background template we were able to reduce our sensitivity to the interfering Auger peaks by ~50%. Even so, we found the scatter to be ~10%, or four times worse than the statistical uncertainty in the Gaussian peak. Peak area normalization is the second step in data reduction. In some previous work[1,2] we have

estimated normalization factors from the inelastic electron background. Since the background, constituting over half the "signal" in each spectrum, is caused by inelastic scattering of much higher energy Auger electrons and photoelectrons, we should be able to relate the background intensity to the cross section for producing the high energy electrons and also to the incident photon flux. Typically the relation between the background intensity and the photon flux varies smoothly over the ARPEFS energy range. The S/Mo background, however, has substantial contributions from Mo LMM Auger electrons; when we scan through the Mo 2s and $2p_{1/2}$ edges, the background is enhanced significantly, thus invalidating the background as a reference. We were forced to resort to an external photon flux monitor situated between the monochromator and the sample. This Ni grid -- channeltron assembly measures the relative photon flux incident on the grid wires, but the ratio between the apparent incident flux and useful flux (light illuminating the sample at the spectromter focus) changes with the photon beam intensity profile. The intensity profile changes when the storage ring is refilled with electrons. Depending on storage ring conditions, a fill may be required as often as once every 5-10 hours. Inadequate steering control also distorts the intensity profile occasionally. By combining "background" and "flux" normalization, we were able to accomodate both the Mo absorption edges and various beam effects to obtain complete ARPEFS curves.

The data reduction is then concluded by removing an atomic-like background (I_0), typically determined as a low-order polynomial fitted to the I(E) curve. This final step follows the relation

$$\chi(k) = \frac{I-I_0}{I_0}$$

where $\chi(k)$ is the modulation of the photoelectron intensity caused by the PD effect. The removal of a polynomial I_0 is somewhat arbitrary because of competing effects of analyzer transmission and uncertain photoemission partial cross-section. The I_0 removal will necessarily remove additional low frequency signal, if present, from the χ curve. The derived χ curves are shown in Figs. 3 and 4. The 0° curve labeled "#1" in Fig. 3 was measured from a sample probably having greater disorder than that for curve #2, which accounts for the difference in amplitude. Despite the interfering Auger peaks and the difference in surface order, the two 0° curves agree fairly well otherwise. In comparison, the 35° curves in Fig. 4 appear quite noisy. In part, this is because the 35° χ amplitude is lower than 0° χ amplitude. Also, the measurement time was reduced for the 35° curves so the experiment could be concluded in the remaining beam time. The 35° curves agree fairly well in two aspects: the amplitude is similar and the averaged curve agrees with the individual curves in most details, at least within the scatter of the data.

IV. Structural Analysis

We have determined the structure of S/Mo using two methods of ARPEFS data analysis. The first, Fourier transformation, provides a semi-quantitative path-length difference distribution of the scattering

atoms. The second, fitting of data with multiple-scattering spherical-wave (MSSW) theory is quantitative and can provide detailed structural parameters of the adsorption site.

The first method, involving Fourier analysis, is analogous to the extended x-ray absorption fine-structure (EXAFS) Fourier analysis method.[11] We have found that in certain geometries, the positions of the Fourier peaks can be used to ascertain the adsorption geometry directly.[2,12] The S/Mo data were Fourier transformed using methods previously described.[1,2] These transforms are plotted in Fig. 5 as peaks in path-length difference space.

The 0° transform is easy to understand because the emission angle has high symmetry and because the data are dominated with relatively few frequencies. If we approach the 0° transform with no detailed knowledge of the molybdenum surface, we can extract a crude structure rather easily. First, based on sulfur adsorption to other fourfold symmetric metal surfaces, we would expect the sulfur atom to bond at the fourfold hollow site of Mo(001). The hollow site is rather shallow, however, and a reasonable S-Mo bond distance would predict a sulfur-to-second layer Mo distance fairly similar (within 0.2Å) to the S-Mo bond distance. This raises the possibility of a fivefold S-Mo surface bond. Continuing from the assumption that the bonding site is the fourfold hollow, we can proceed to assign the Fourier peaks. We would assign the first peak-shoulder at 3.0Å as a geometrical path-length difference, corresponding to scattering from the nearest-neighbor Mo atoms. The 3.0Å path-length difference implies a S-Mo bond distance of about 2.3Å, or a S-Mo(1) layer spacing of 0.7Å. This low-frequency peak is somewhat influenced by the choice of background I_0

functions, so we cannot quote the S-Mo bond distance with confidence, based on the Fourier analysis alone.

The 4.4Å peak can then be described with scattering from the nearest-neighbor sulfur atoms, which, for a perfect c(2X2) overlayer, would have a path-length difference of 4.44Å. The 4.4Å peak also contains substantial contributions from double-scattering events involving the nearest-neighbor Mo atoms and the nearest-neighbor S atoms. The next peak-shoulder at 5.2Å corresponds to major scattering contributions from the second-layer Mo atom directly below the S emitter. The 5.2Å path-length difference would imply a S-Mo(2) spacing of 2.6Å. Other third- and fourth-layer Mo scattering atoms have path-length differences close to observed peaks, as shown in Fig. 5.

The 0° transform results agree surprisingly well with a simple structural model for S/Mo, and with this Fourier analysis we predict a 2.3Å S-Mo bond distance and a 1.9Å Mo first-to-second layer spacing. The major peak structures are easily explained with only a few scattering atoms with path-length differences corresponding to sulfur adsorption in the fourfold hollow site. This result requires minimal theoretical input, and additionally provides a fairly accurate S-Mo bond distance of about 2.3Å (comparing the Fourier analysis result with the results obtained from the MSSW fits, described later in this section). We would generally expect the Fourier peaks to be shifted and otherwise distorted by the scattering phase shifts and the contributions of additional inequivalent scattering atoms. In this case, we find empirically that a simple Fourier analysis provides crude, but useful, structural information.

The 35° Fourier transform is difficult to describe with only a few path lengths because the symmetry is much lower than that for the 0° data and consequently there are many inequivalent scattering atoms at similar frequencies. The 35° transform also has a rather high noise level relative to the signal. We will not attempt to assign the 35° transform peaks.

At least for higher path-length differences in high-symmetry directions, we find that Fourier analysis can provide useful structural information, with the caveat that peaks are sometimes distorted by the scattering phase shift and by additional contributions from similar path-length scattering atoms. Without correcting for these interfering effects, we cannot expect to gain more than semi-quantitative information. In summary, we find that the Fourier transform analysis is consistent with a fourfold hollow site, a S-Mo bond distance of about 2.3Å, and a Mo(1)-Mo(2) layer spacing of about 1.9Å.

The second, more quantitative, method of analysis, also described previously,[1,2] is the fitting of MSSW theory[13-15] to the data. The basic aspects of the theory specific to different types of scattering atoms and surfaces are the Debye-Waller temperatures (for thermal disorder effects) and the partial-wave phase shifts (for the complex scattering amplitude).

We selected the z-axis bulk and surface Mo Debye temperatures from the LEED work of Tabor[16] as 380K and 239K, respectively. The sulfur z-axis Debye temperature of 372K was selected by arbitrarily giving sulfur the same mean-squared displacement as the top Mo layer and then correcting for the mass difference. The structural results obtained

from our fits remained constant over a wide range (±50K) of Debye temperatures.

The phase shifts for S and Mo were calculated using a modified version of a program developed by Pendry.[17] The Mo potential was obtained from the self-consistent LDA calculations of Moruzzi et al.[18] The S phase shifts were calculated using a potential obtained from Hartree-Fock wavefunctions as in the work of Robey et al.[19] Phase shifts were calculated for ℓ=0 to 19 over the energy range ~50-550 eV. The plane-wave scattering-amplitude magnitude for Mo, calculated from these phase shifts, is shown in Fig. 6, plotted in polar form for several scattering energies. The zeros in scattering amplitude at several angles and energies are Generalized Ramsauer-Townsend (GRT) resonances,[20-21] and are associated with rapid changes in the total phase shifts. The peak for 180° scattering is largely responsible for the emphasis on atoms directly opposite the emitter from the detector. The dominant 0° scattering peak is responsible for the importance of forward scattering. Taken together, the 0° and 180° peaks emphasize events involving backscattering plus multiple forward scattering. Since forward scattering introduces only a small phase shift, the amplitudes of oscillations in $\chi(k)$ caused by these events are enhanced by the subsequent forward scattering.

The MSSW fitting method of analysis follows an algorithm described previously.[2] We compute the χ^2 error between the data and theory for different model geometries. If we consider the range of valid atomic coordinates to be a multidimensional, non-linear least-squares parameter space, we can locate a minimum in χ^2 and estimate the uncertainty in each associated atomic coordinate. We began our

minimization by calculating for the three simplest adsorption sites. Calculations for the three adsorption sites -- bridge, atop, and fourfold hollow -- are shown in Figs. 7 and 8, compared with the experimental curves. The fourfold hollow calculations are clearly in best agreement with the experimental curves, although the fits are far from excellent, in part because the geometries are not optimized. Starting from the fourfold site, we varied the S-Mo(1), S-Mo(2), and S-Mo(3) vertical positions from the ideal bulk-equivalent positions. We also allowed the "covered" Mo(2c) atoms to have different vertical positions than the "open" Mo(2o) atoms. For the 35° data, the emission angle was also varied (rotated 0.4° away from the surface normal and 2° out of the [001], [111] plane) to improve the fit. The results of these fits are shown in Figs. 3 and 4, where the thick lines are the calculations for the optimized structure.

The structural results are listed in Table 1. The S-Mo(1) distance was optimized at 0.93(4)Å, which implies a S-Mo bond distance of 2.41(2)Å. The S-Mo(2c) distance was optimized at 2.55(3)Å, implying a Mo(1)-Mo(2c) separation of 1.62(5), which is within one standard deviation of the bulk spacing of 1.57Å. The second Mo layer was allow to buckle, but it appeared to be planar with an uncertainty of 0.03Å. The Mo(2c)-Mo(3) spacing was optimized at 1.57(7)Å, essentially bulk-like. We also quote a highly precise Mo-S-Mo surface bond angle of 134.5(5)°.

V. Discussion

The results we have presented illustrate the sensitivity of ARPEFS to the geometry of an adsorption site. The level of structural determination we have achieved in this case was limited by systematic errors (Auger peaks) and random noise (counting statistics) in the data.

The confidence with which we assign the positions of atoms near sulfur is determined by two factors: the statistical precision for a variable parameter which we determine from the MSSW fits, and the generality of our structural model. The uncertainties which we quote in Table 1 are valid to the extent that the local structure near the sulfur emitter fits our model. As we described in detail in Section IV, our model allowed variations of the vertical positions of the top three Mo layers relative to S, with independent relaxation of inequivalent second-layer Mo atoms. The observed c(2X2) LEED pattern restricts the surface symmetry but not the orientation of surface atoms relative to the bulk. However, we do not find evidence in our data for lateral reconstruction of the top Mo layer, although the possibility was suggested by Clarke.[8]

The relaxation of the Mo surface from a 13% contracted first-to-second layer spacing, in the case of clean Mo,[4] to a nearly bulk-like first-to-second layer spacing for sulfur-covered Mo, determined in this work, corresponds to a change in the surface Mo-Mo bond distance from 2.61Å to 2.74(3)Å, an increase of 5%.

The measured S-Mo bond distance agrees well with a bond distance estimated as the sum of the sulfur covalent radius of 1.03Å[22] and one-half the molybdenum bulk nearest-neighbor separation of 2.725Å/2. The

covalent-metallic bond distance would be 2.39Å, compared with our measured value of 2.41(2)Å.

Acknowledgements

This work was supported by the Director, Office of Energy Research, Office of Basic Energy Sciences, Chemical Sciences Division of the U.S. Department of Energy under Contract No. DE-AC03-76SF00098. It was performed at the Stanford Synchrotron Radiation Laboratory, which is supported by the Department of Energy, Office of Basic Energy Sciences. One of us (Z.H.) acknowledges support by the University of Petroleum and Minerals under project number PHYS/APRES/71.

* Permanent address: Department of Physics, University of Petroleum and Minerals, Dhahran, Saudi Arabia.

Table 1. Structural parameters (in Angstroms) determined for c(2X2)S/Mo(001), with uncertainties in parenthesis. Multiple-scattering spherical-wave (MSSW) calculations were optimized to agree with the data by varying the positions of Mo atoms near the S emitter.

parameter	0°	35°	average
S-Mo(1)[a]	0.94(4)	0.91(7)	0.93(4)
S-Mo(2c)[a]	2.54(2)	2.56(5)	2.55(3)
S-Mo(2o)[a]	2.54(9)	2.68(16)	2.57(9)
S-Mo(3)[a]	4.12(5)	4.05(10)	4.11(6)
S-Mo[b]			2.41(2)
Mo(1)-Mo(2c)[b]			1.61(5)
Mo(2c)-Mo(3)[b]			1.57(7)
<(Mo-S-Mo)[b]	134	135	134.5(5)

[a] Extracted directly from fits of MSSW theory to data.

[b] Indirectly derived from measured parameters.

References

1. J.J. Barton, C.C. Bahr, S.W. Robey, Z. Hussain, E. Umbach, and D.A. Shirley, Submitted to Phys. Rev. B.
2. C.C. Bahr, J.J. Barton, Z. Hussain, S.W. Robey, J.G. Tobin, and D.A. Shirley, submitted to Phys. Rev. B.
3. A.J. Gellman, M.H. Farias, M. Salmeron, and G.A. Somorjai, Surf. Sci. 136, 217 (1984).
4. A. Ignatiev, F. Jona, H.D. Shih, D.W. Jepsen, and P.M. Marcus, Phys. Rev. B 11, 4787 (1975).
5. T.E. Felter, R.A. Barker, and P.J. Estrup, Phys. Rev. Lett 38, 1138 (1977).
6. A. Ignatiev, F. Jona, D.W. Jepsen, and P.M. Marcus, Phys. Rev. B 11, 4780 (1975).
7. B.M. DeKoven, S.H. Overbury, and P.C. Stair, J. Vac. Sci. Technol. A3, 1640 (1985).
8. L.J. Clarke, Surf. Sci. 102, 331 (1981).
9. Z. Hussain, E. Umbach, D.A. Shirley, J. Stöhr, J. Feldhaus, Nucl. Inst. Methods 195, 115 (1982).
10. S.D. Kevan, Ph.D. Thesis, University of California, Berkeley, (1980).
11. G. Martens, P. Rabe, N. Schwentner, and A. Werner, Phys. Rev. B 17, 1481 (1978).
12. J.J. Barton, C.C. Bahr, Z. Hussain, S.W. Robey, J.G. Tobin, L.E. Klebanoff, and D.A. Shirley, Phys. Rev. Lett. 51, 272 (1983).
13. J.J. Barton and D.A. Shirley, Phys. Rev. A 32, 1019 (1985).

14. J.J. Barton and D.A. Shirley, Phys. Rev. B 32, 1906 (1985).

15. J.J. Barton and D.A. Shirley, Phys Rev B 32, 1892 (1985).

16. D. Tabor, J.M. Wilson, and T.J. Bastow, Surf. Sci 26, 471 (1971).

17. J.B. Pendry, Low Energy Electron Diffraction. (Academic Press, London, 1974).

18. V.L. Moruzzi, J.F. Janak, A.R. Williams, Calculated Electronic Properties of Metals, (Pergamon Press, New York, 1978).

19. S.W. Robey, J.J. Barton, C. C. Bahr, G. Liu, and D. A. Shirley, Submitted to Phys. Rev. B.

20. J.J. Barton, C.C. Bahr, Z. Hussain, S.W. Robey, L.E. Klebanoff, and D.A. Shirley, Proceedings for the Brookhaven Conference, Advances in Soft X-ray Science and Technology, S.P.I.E. v. 447, 82 (1984).

21. M. Sagurton, E.L. Bullock, and C.S. Fadley, Phys. Rev. B 30, 7332 (1984).

22. F.A. Cotton, G. Wilkinson, Advanced Inorganic Chemistry, 421 (John Wiley & Sons, New York, 1972).

Figure Captions

Figure 1. Side views of the S/Mo surface are shown, with slices taken perpendicular to the [100] and [101] directions, as shown.

Figure 2. These electron spectra illustrate the interference of Auger peaks with the photoemission peak. Each spectrum here contains the sulfur 1s peak, which is roughly centered in each window. Additional peaks are Mo MNN Auger transitions.

Figure 3. Two normal emission (0°, along [001]) ARPEFS curves (thin lines connecting the dots) are plotted as a function of electron kinetic energy. The bottom curve (#1) corresponds to a sample with a higher degree of disorder than the top curve. The thick solid lines are optimized MSSW theory, unscaled in curve #2, and scaled by 1/2 in curve #1. Positions of interfering S and Mo Auger peaks are shown as solid bars at the bottom, and the thresholds for Mo $2p_{1/2}$ and 2s emission are shown at the top.

Figure 4. The 35° off-normal (35° from [001] towards [111]) ARPEFS curves are shown in plots #1 and #2. The average of these is shown at the top as a thin solid line. The best fit of theory to data is also plotted at the top as a thick solid line. The maximum diffraction amplitude was less than 1/2 that of the 0° data.

Figure 5. The Fourier transforms of the 0° curve #2 and the 35° average curve are shown plotted as a function of the scattering path-length difference. Geometrical path-length differences for selected scattering atoms are indicated on the 0° transform.

The labels "(1)" through "(4)" refer to Mo atoms in layers 1-4 which scatter near 180°. The largest peak in the 0° transform, which occurs at 4.4Å, is caused by single-scattering at 90° from nearest-neighbor S atoms and multiple-scattering involving the nearest-neighbor S atoms and nearest-neighbor Mo atoms.

Figure 6. A polar plot of the plane-wave scattering amplitude for Mo is shown for three energies, k= 5, 9, and 12 $Å^{-1}$. Generalized Ramsauer-Townsend resonances occur at energies and angles where the scattering amplitude sweeps through zero.

Figure 7. Three MSSW calculations are shown for ideal (non-optimized) fourfold hollow, atop, and bridge bonding sites for c(2X2)S/Mo(001), assuming a S-Mo bond distance of 2.40Å and an unrelaxed Mo surface. The curves are calculated for the 0° experimental geometry. The data curve shown is the 0° curve #2, from Fig. 3.

Figure 8. Three MSSW calculations are shown, as in Fig. 7, but for the ideal (non-optimized) 35° geometry. The data shown here are averaged data from Fig. 4.

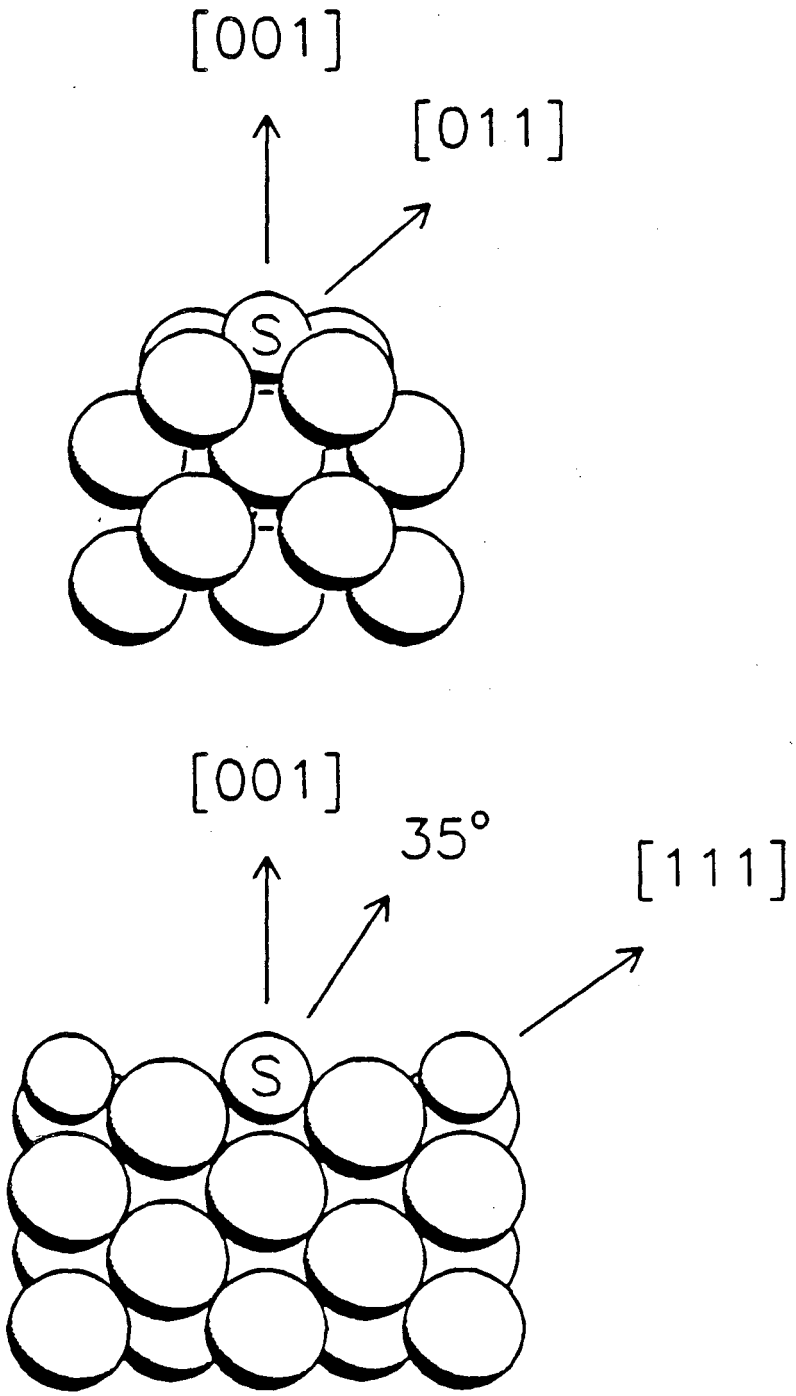

XBL 863-1026

Figure 1

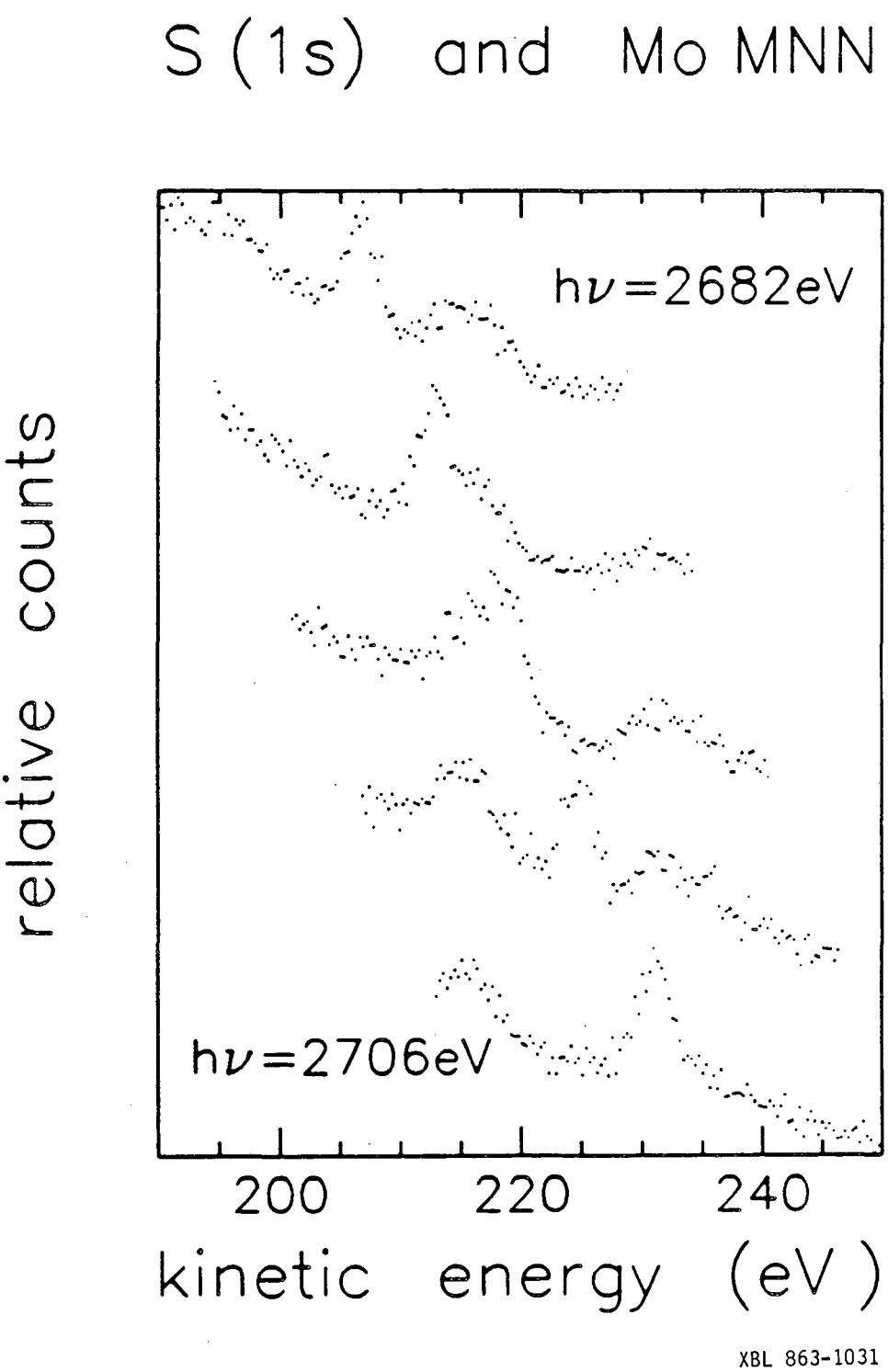
S (1s) and Mo MNN
hν=2682eV
hν=2706eV
relative counts
200
220
240
kinetic energy (eV)
XBL 863-1031

Figure 2

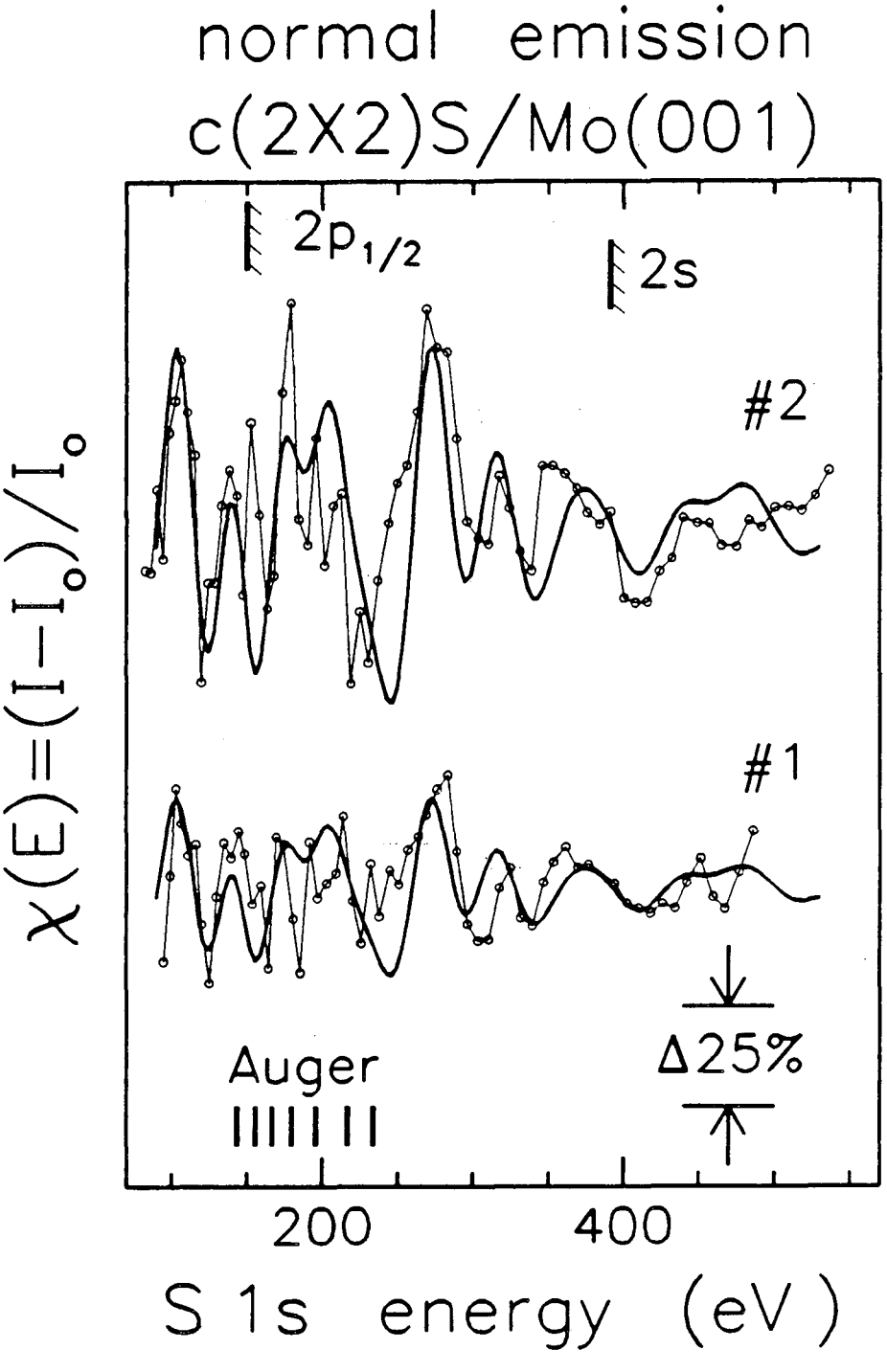

XBL 863-1027

Figure 3

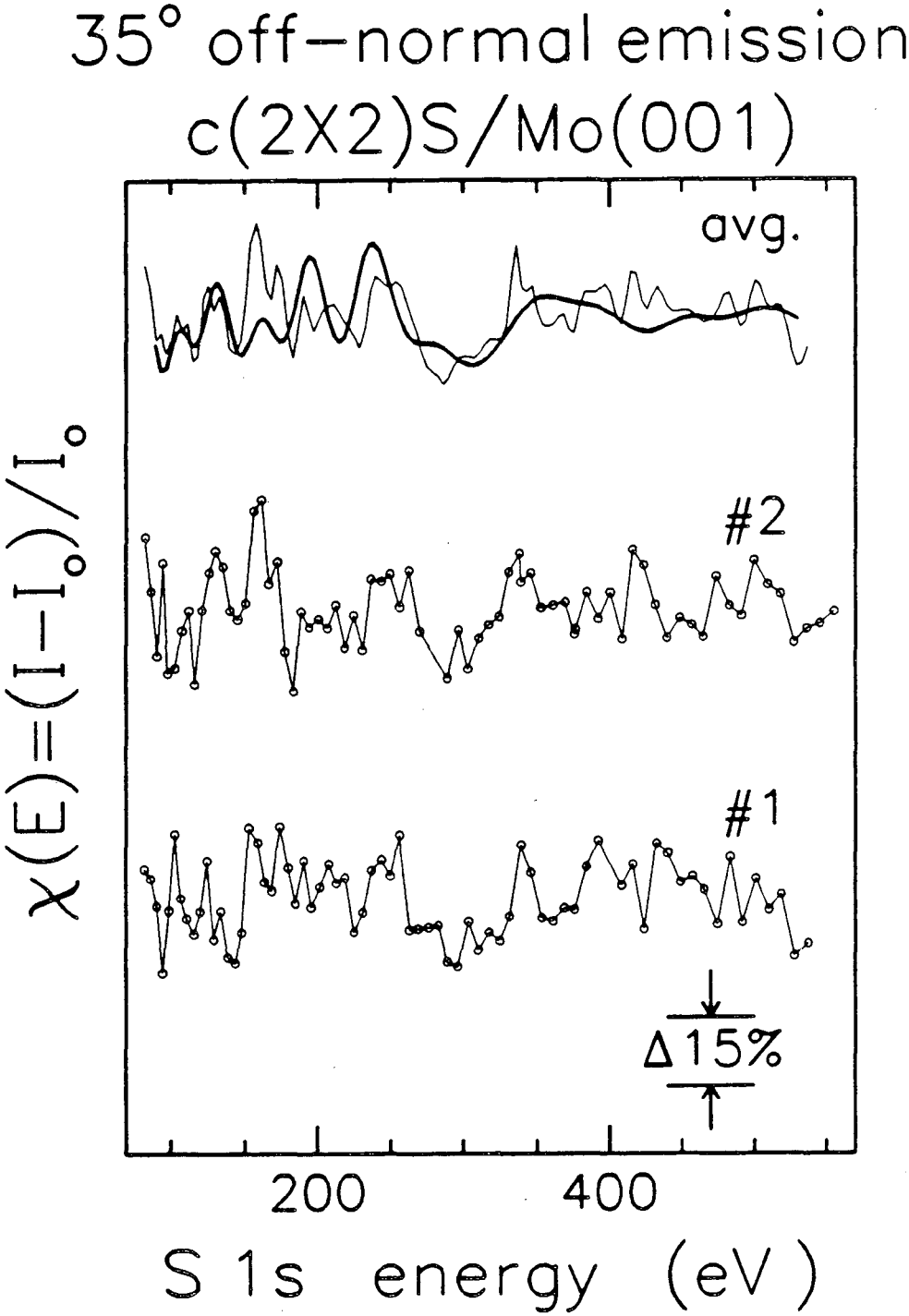
35° off-normal emission
c(2X2)S/Mo(001)
avg.
#2
#1
Δ15%
χ(E)=(I−I₀)/I₀
200
400
S 1s energy (eV)
XBL 863-1028

Figure 4

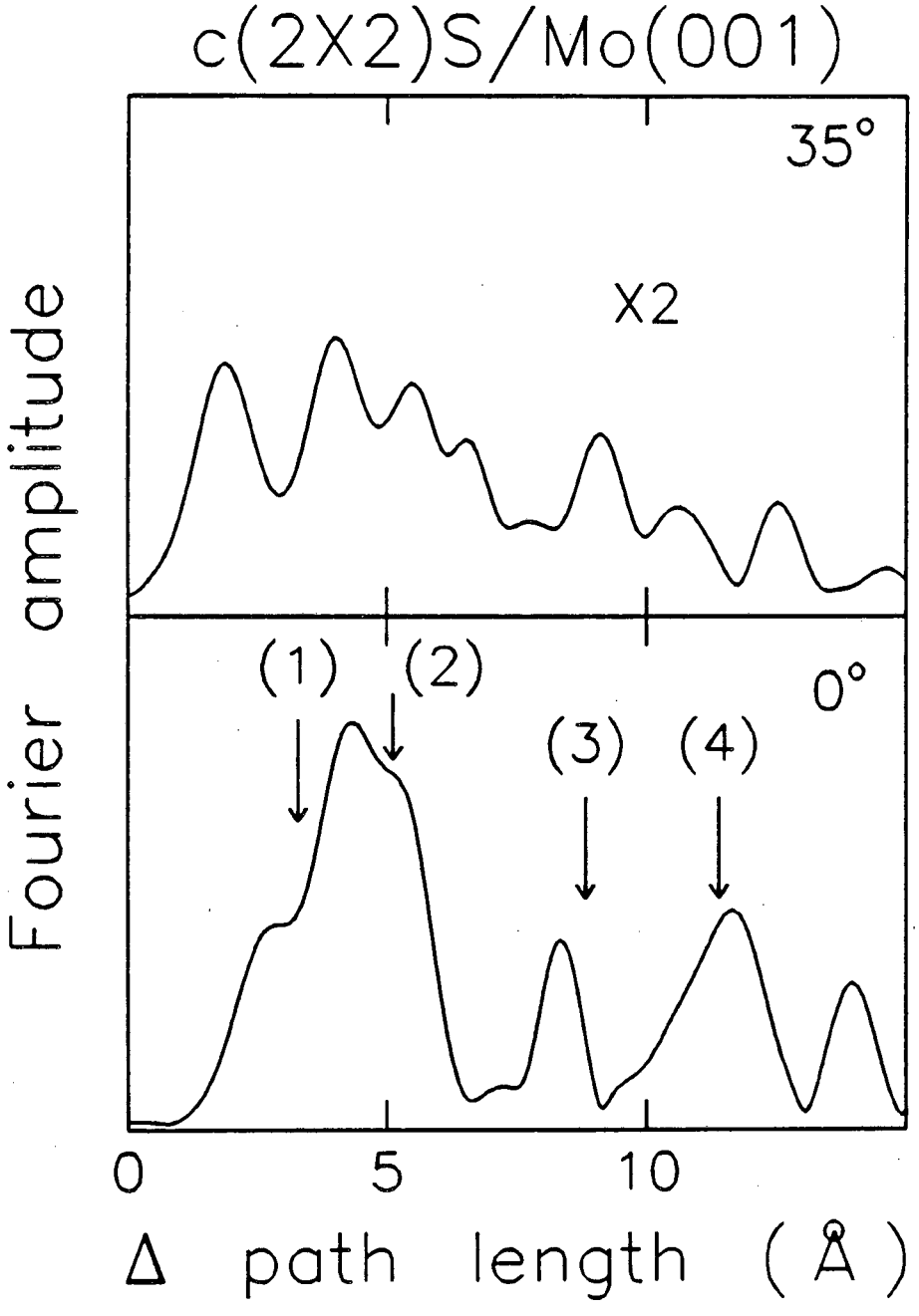

XBL 864-1237

Figure 5

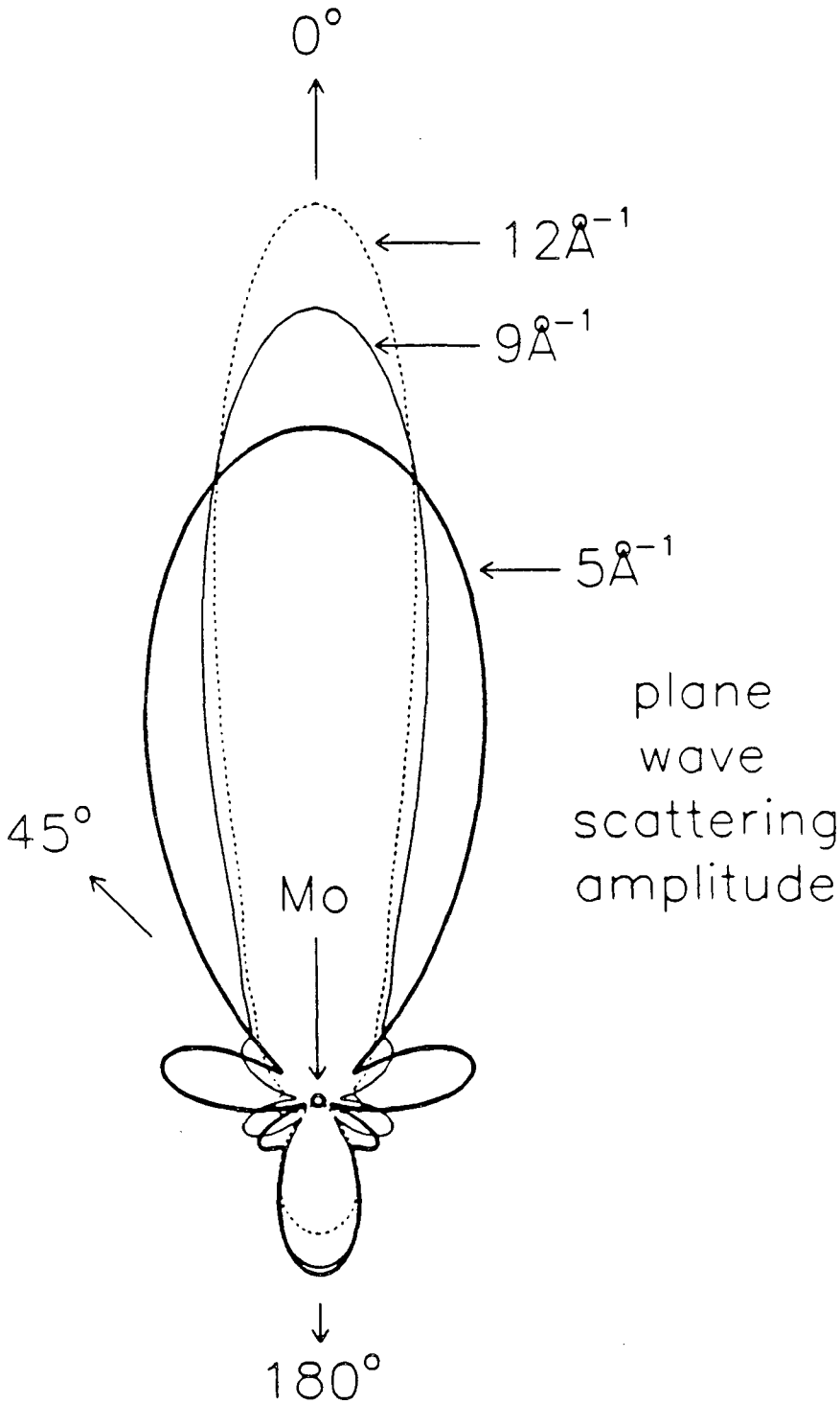
0°
12Å^{-1}
9Å^{-1}
5Å^{-1}
plane
wave
scattering
amplitude
45°
Mo
180°
XBL 863-1025

Figure 6

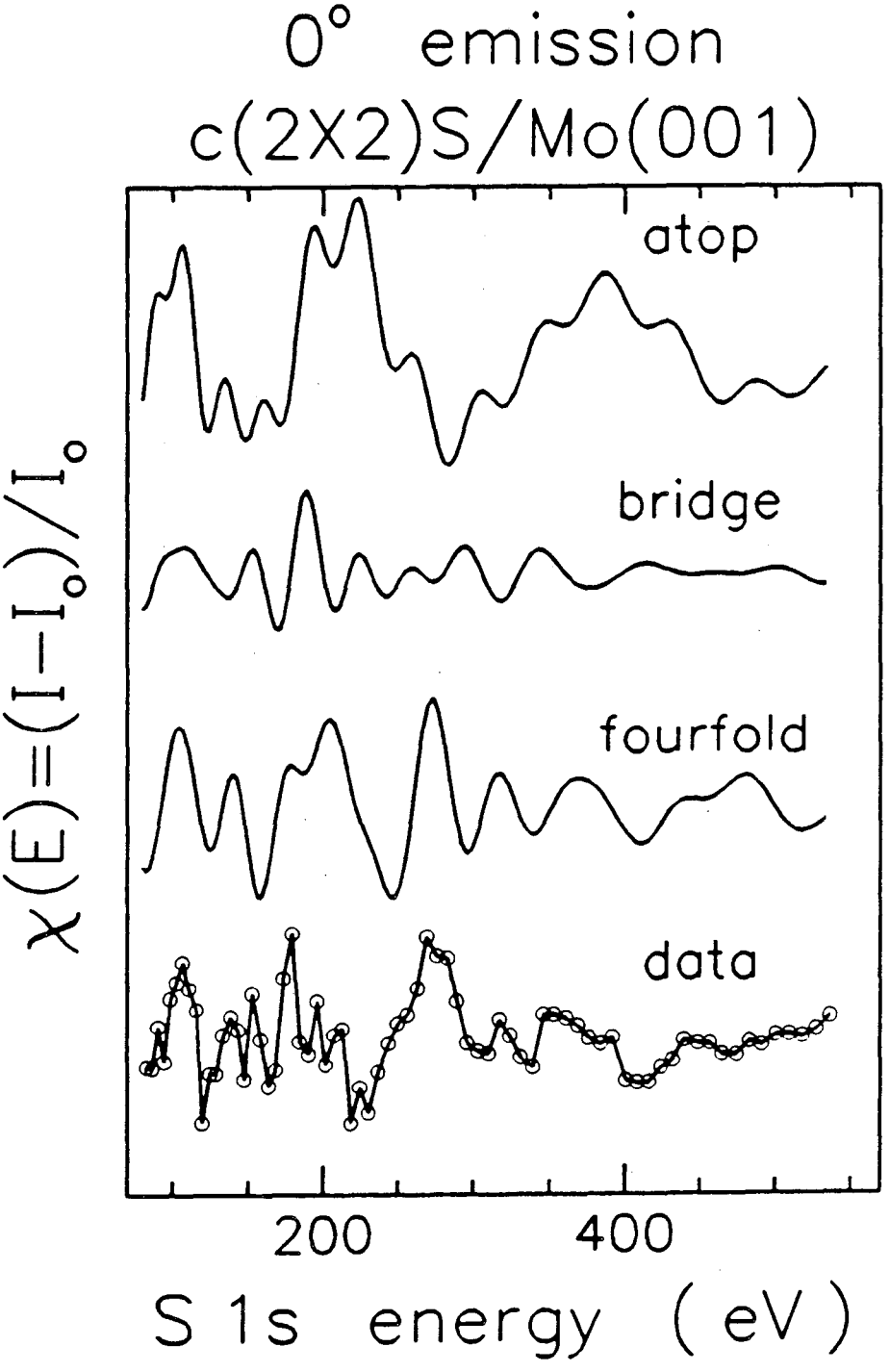

XBL 863-1029

Figure 7

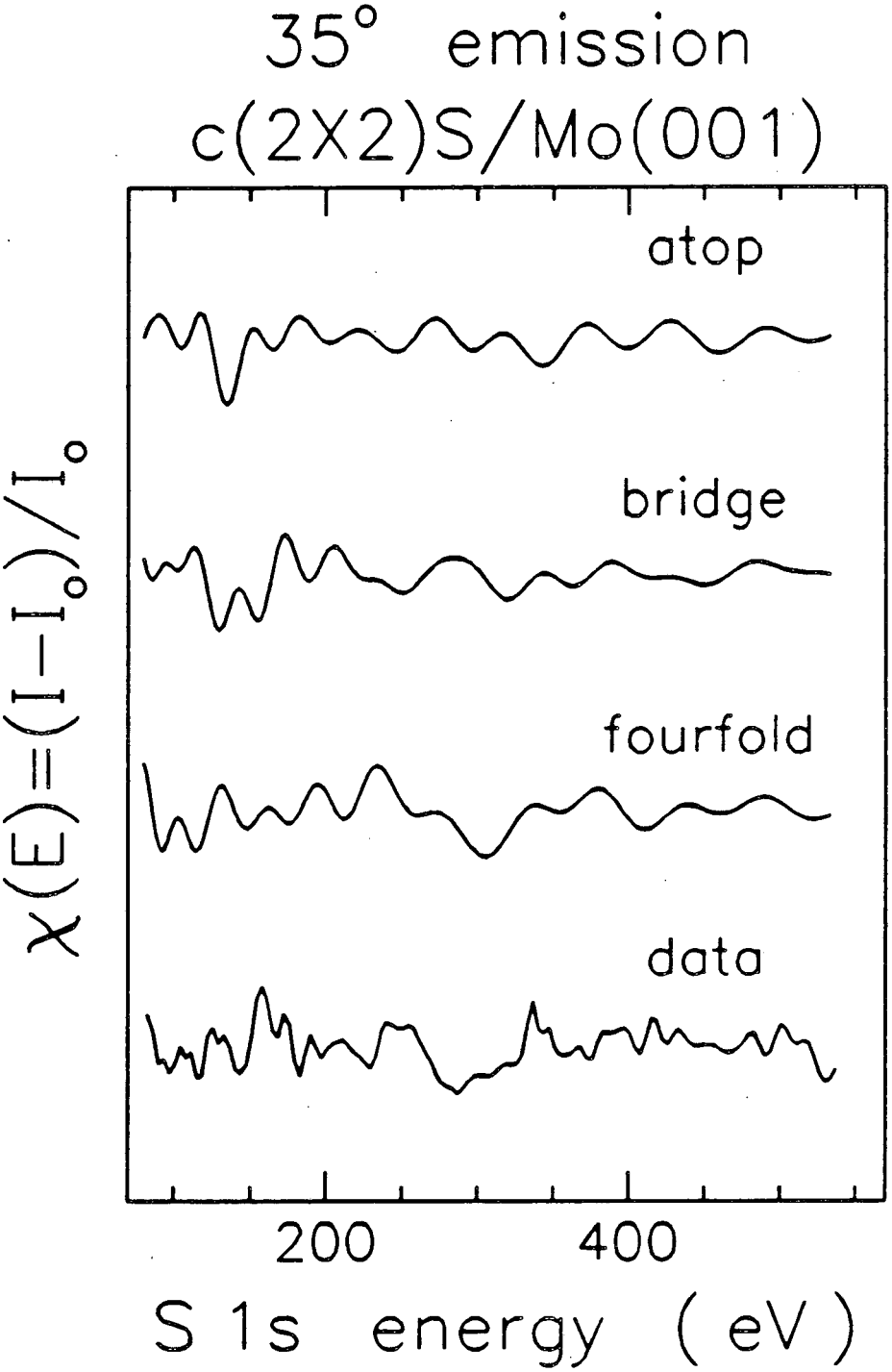
35° emission
c(2X2)S/Mo(001)
atop
bridge
fourfold
data
χ(E)=(I−I₀)/I₀
200
400
S 1s energy (eV)
XBL 863-1030

Figure 8

LAWRENCE BERKELEY LABORATORY
TECHNICAL INFORMATION DEPARTMENT
UNIVERSITY OF CALIFORNIA
BERKELEY, CALIFORNIA 94720